HAL
open science

Monolithic Double Resonator for Quartz Enhanced Photoacoustic Spectroscopy

Roman Rousseau, Diba Ayache, Nicolas Maurin, Wioletta Trzpil, Michaël Bahriz, Aurore Vicet

To cite this version:

Roman Rousseau, Diba Ayache, Nicolas Maurin, Wioletta Trzpil, Michaël Bahriz, et al.. Monolithic Double Resonator for Quartz Enhanced Photoacoustic Spectroscopy. Applied Sciences, 2021, 11 (5), pp.2094. 10.3390/app11052094 . hal-03260067

HAL Id: hal-03260067

https://hal.science/hal-03260067v1

Submitted on 14 Jun 2021

HAL is a multi-disciplinary open access archive for the deposit and dissemination of scientific research documents, whether they are published or not. The documents may come from teaching and research institutions in France or abroad, or from public or private research centers.

L'archive ouverte pluridisciplinaire **HAL**, est destinée au dépôt et à la diffusion de documents scientifiques de niveau recherche, publiés ou non, émanant des établissements d'enseignement et de recherche français ou étrangers, des laboratoires publics ou privés.

applied sciences

MDPI

Article

Monolithic Double Resonator for Quartz Enhanced Photoacoustic Spectroscopy

Roman Rousseau, Diba Ayache, Nicolas Maurin, Wioletta Trzpil, Michael Bahriz and Aurore Vicet *

IES, University Montpellier, CNRS, 34090 Montpellier, France; roman.rousseau@ies.univ-montp2.fr (R.R.); diba.ayache@ies.univ-montp2.fr (D.A.); nicolas.maurin@ies.univ-montp2.fr (N.M.); Wioletta.Trzpil@ies.univ-montp2.fr (W.T.); michael.bahriz@umontpellier.fr (M.B.)

* Correspondence: aurore.vicet@umontpellier.fr

Abstract: A new approach for Quartz Enhanced Photoacoustic Spectroscopy is presented, based on an acoustic excitation from the outside of the prongs of a quartz tuning fork, to increase the sensitivity of the sensor. For this purpose, we introduce a monolithic acoustic double-resonator (double-mR) in a T-shape configuration, using 3D printing. It was modelized and experimentally characterized using a 1392 nm distributed feedback laser diode, targeting a water vapor absorption line. The setup showed a two-factor enhancement of the signal, compared to a classical off-beam QEPAS approach and confirmed the strong interest of photolithographic printing techniques for acoustic developments.

Keywords: photoacoustics; infrared; laser; sensing; QEPAS

Citation: Rousseau, R.; Ayache, D.; Maurin, N.; Trzpil, W.; Bahriz, M.; Vicet, A. Monolithic Double Resonator for Quartz Enhanced Photoacoustic Spectroscopy. *Appl. Sci.* **2021**, *11*, 2094. https://doi.org/10.3390/app11052094

Academic Editor: Bernhard Wilhelm Roth

Received: 27 January 2021
Accepted: 23 February 2021
Published: 26 February 2021

Publisher's Note: MDPI stays neutral with regard to jurisdictional claims in published maps and institutional affiliations.

Copyright: © 2021 by the authors. Licensee MDPI, Basel, Switzerland. This article is an open access article distributed under the terms and conditions of the Creative Commons Attribution (CC BY) license (http://creativecommons.org/licenses/by/4.0/).

1. Introduction

Gas sensing is strongly demanding on sensitive, selective, and efficient techniques, to be implemented on laboratories experiments, environmental, medical, or industrial purposes. Since its invention in 2002 [1], Quartz Enhanced Photoacoustic Spectroscopy (QEPAS) demonstrated many advantages among techniques based on tunable sources and indirect gas absorption detection.

Photoacoustic spectroscopy relies on light absorption, through a specific gaseous species, when an absorption line corresponds to the emitted wavelength of a source. The source can be a laser or a broader source such as a light emitting diode [2]. While the source intensity is modulated, the light absorption is modulated as well, and gives rise to a localized sound wave at the modulation frequency. This indirect photonic effect is called the photoacoustic effect, which has been exploited for years [3], using resonant acoustic cells and microphones for sound sensing. In QEPAS, the sound wave interacts with a mechanical transducer (a quartz tuning fork or QTF), leading to a piezoelectric current. Thanks to the very high quality factor of the QTF (~10,000 at atmospheric pressure), it is unnecessary to use any resonant acoustic cell, as done in classical microphone photoacoustics sensing.

In order to enhance the pressure wave amplitude, some small tubes called micro-resonators (mR) can be added to the optical setup, leading to two main configurations (on-beam/off-beam). In the on-beam configuration [4], the resonator tubes are placed on both sides of the QTF plane, leaving a small air gap (<100 μm) with the QTF prongs. In the off-beam configuration [5], the resonator tube is located on one side of the QTF, in the center alongside the prongs. On-beam QEPAS exhibits a good signal enhancement factor of around 30 [6,7], but it requires a stringent optical alignment to avoid photothermal effects, due to direct illumination of the QTF. Standard commercial QTF are not adapted to long wavelength sources such as quantum cascade lasers because of the small gap (0.3 mm) between the prongs, leading to the development of large custom QTF, first for THz

sensing [8,9], and their successful use in several applications. Despite a smaller signal enhancement, the off-beam configuration reduces optical constraints, gives more flexibility to the setup developments, and can be competitive in terms of sensitivity with on-beam QEPAS. This configuration was studied theoretically [10] and successfully implemented in molecular spectroscopy, for many purposes [11–15].

The two QTF prongs move symmetrically and are best coupled with a cylindrical acoustic wave, when the longitudinal axis of the wave is located in between the two prongs. Both on-beam and off-beam satisfy this condition—one acoustic source symmetrically acting on the inner surface of both prongs. Alternatively, the QTF can be excited by applying a force on the external surface of both prongs, but it requires two acoustic sources. We rethought the design of the spectrophone to be able to excite the QTF from the outside of the two prongs.

A comparable approach was realized at the same time by Hu and Al [16,17]. This design was based on a QTF-embedded, double-pass, off-beam spectrophone. Similar to the original off-beam mR [5], the spectrophone is made of two cylindrical mRs with a slit in the center. The QTF is embedded in the mRs, the slit is large enough to partly immerse the QTF prong inside the mR cavity. In this configuration, two acoustic sources (from the two mRs) were employed to excite the external surfaces of the prongs.

The novelty of our approach relied on a monolithic double-resonator (double mR) in a T-shape configuration, 3D-printed (stereolithography = SLA) characterized, and modelized, thanks to our experience on single resonator evaluation [15]. In this paper, we pre-sent this new configuration, its design, characterization, and evaluation, using an open-air QEPAS configuration dedicated to ambient water vapor sensing with a 1392 nm DFB laser.

2. Experimental Setup

The QEPAS spectrophone was designed to excite the QTF from the outside of the prongs. We used two off-beam mRs placed in a mirror symmetry and the QTF located in between (Figure 1). The optical path was more complex, compared to a classical off-beam QEPAS approach. The laser beam went through one microresonator (mR 1), underwent two right angle reflections that brought it parallel to the incoming beam with a lateral shift (δ), and finally crossed the other microresonator (mR 2).

In this configuration, one could consider two acoustic sources photogenerated with the same laser. In order to maximize the excitation of the QTF, the two acoustic sources must be in-phase. Considering two identical mRs and two identical mR-QTF gaps, the phase shift $\Delta\varphi$ between the two acoustic sources could be calculated with the optical path difference ΔL, between the two mRs:

$$\Delta\varphi = k\Delta L = 1.3 \cdot 10^{-5} \ rad \quad (1)$$

With k as the wave vector, ΔL = 2.2 cm ($2L_{mR} + \delta$ the optical path between the 2 mRs). The phase shift was negligible; therefore, the 2 mRs were considered to be acoustically in phase.

The dimensions of the monolithic double mR were chosen, after the characterization of several individual mR. A set of many different mR with various dimensions, fabricated from aluminum micromachined blocks, were characterized following the setup described in [15]. We chose a large main hole (R_{mR} = 0.5 mm) to help the alignment process. The acoustic response of these individual mRs was studied using a photoacoustic signal generated by the absorption of a water line of a 1392 nm single frequency laser (https://eblanaphotonics.com/ (accessed on 02/26/21)). The laser was fully characterized, as shown in Figure 2.

The target H_2O line had a line strength of 1.5×10^{-20} cm^{-1}/(molecule × cm^{-2}), centered in 1392.54 nm (7181.18 cm^{-1}). The amplitude of acoustic wave, based on a given ambient water absorption (absolute humidity ~1% in volume ratio), corresponded to an optical

absorption coefficient of 1.15 × 10^{-2} cm^{-1}, which was relatively high, as compared to standard gas sensor experiments, but convenient for making a proof of concept.

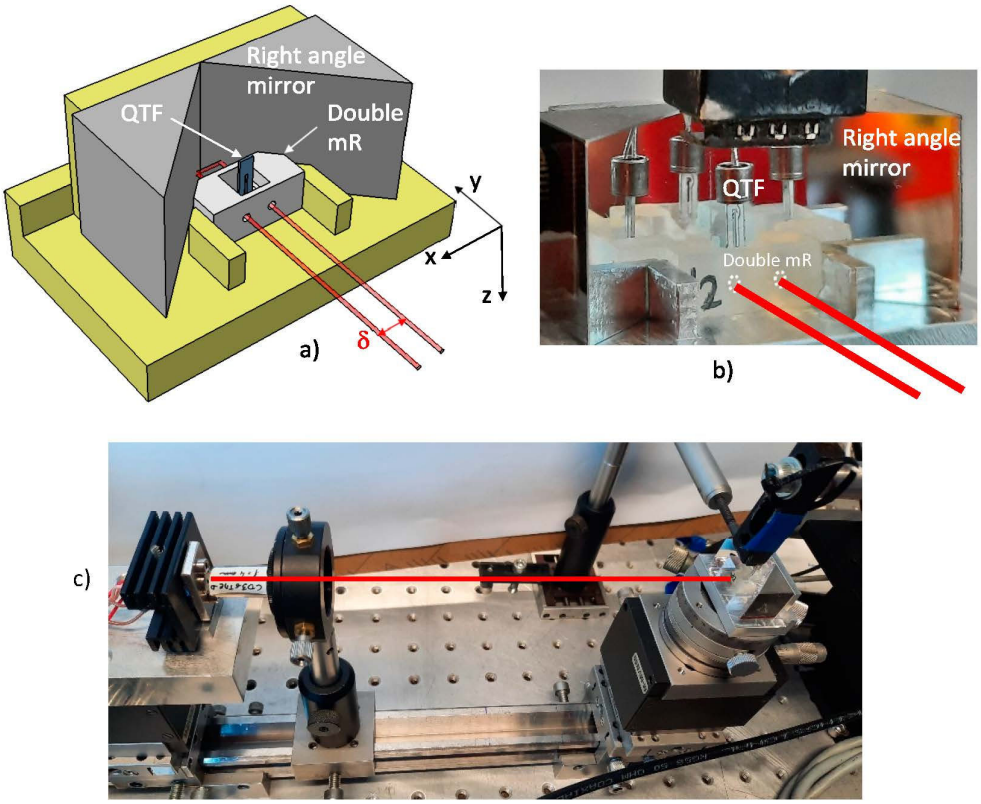

Figure 1. (**a**) Optical QEPAS setup of the double microresonator (double mR) with the 2 right angle mirrors and the QTF position. (**b**) Picture of the setup. (**c**) Picture of the complete bench, including the laser, the focusing lens, and QEPAS spectrophone.

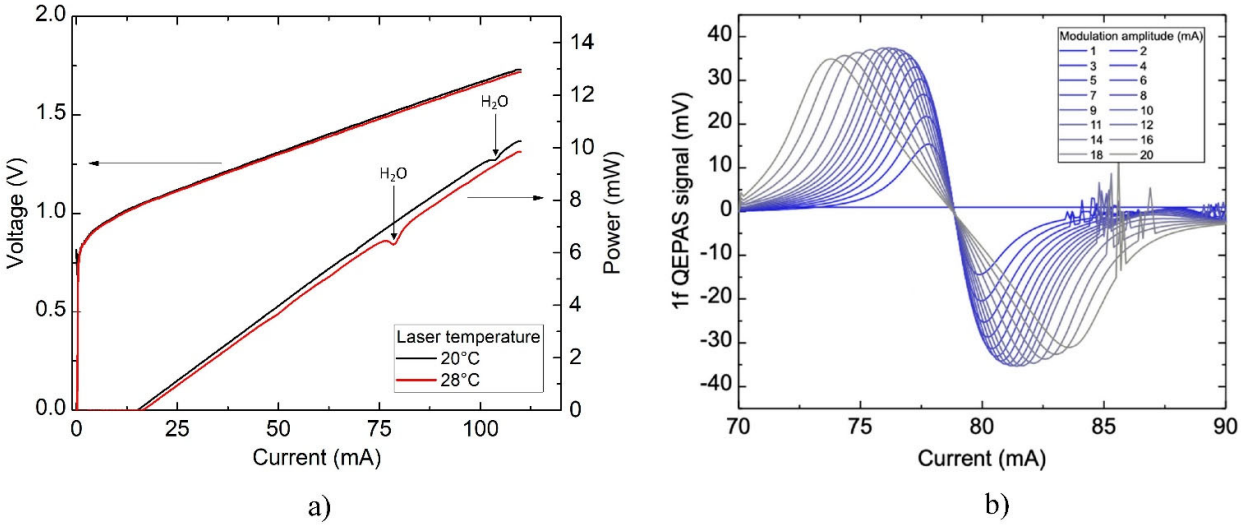

Figure 2. Characteristics of the EBLANA 1392 nm DFB laser. (**a**) LIV curves and (**b**) 1f-QEPAS response in an off-beam configuration with a single microresonator. The spikes at higher currents were due to insignificant experimental artefacts. The QEPAS response was obtained for a laser temperature of 28 °C and ambient humidity of 50% RH.

We used a standard MEMS microphone (Knowles SPU0410LR5H-QB) to record the frequency response of the resonators [15]. These characterizations were conducted using mRs with lengths around $\lambda/2$ for a 2^{15} Hz acoustic wave, adjusted to the theoretical QTF resonant frequency. The best frequency-adjusted response was obtained for a length between 5 and 5.5 mm (Figure 3). We also fabricated 3D stereolithography printed mRs and noticed that changing the material did not modify the resonant properties—the quality factor (Q = 9 for ref a9) and the resonant frequency remained the same. Following these results, we decided to choose L_{mR} = 5.3 mm to fit as properly as possible to the QTF resonant frequency.

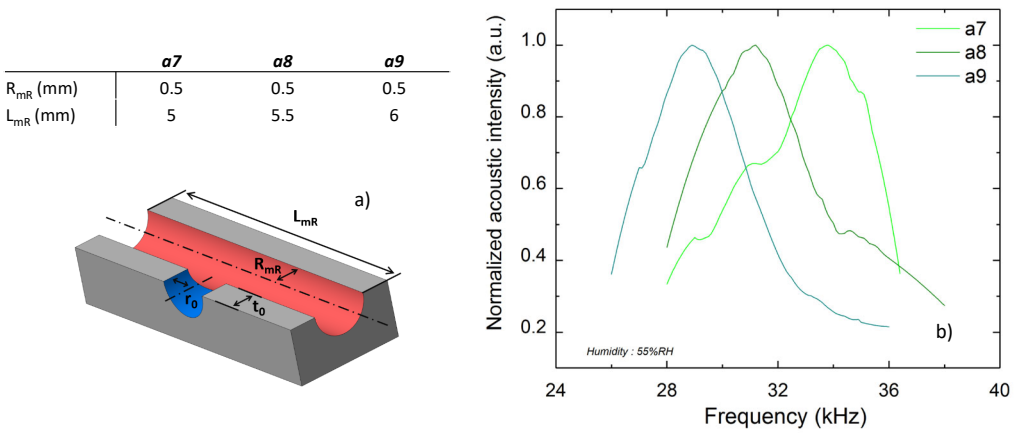

Figure 3. (a) Sectional view and dimensions of 3 mRs a7, a8, and a9, sharing the same radius and different length. r_0 = 0.25 mm, t_0 = 0.3 mm. (b) Normalized experimental acoustic resonance of the 3 resonators.

In this double mR configuration, the two individual mRs were uncoupled, the acoustic wave was mainly confined in the main tube. Its amplitude quickly decreased out of the T tube, as can be seen in Figure 4. To evaluate the normalized sound distribution inside and outside the mRs, a thermo-acoustic frequency analysis of the pressure wave was realized by the finite element method (COMSOL). As predicted by analytical approaches [10,15], the wave was not entirely confined into the tube—about 30% of the total pressure extended outside due to the open ends effect and because of the T-shape.

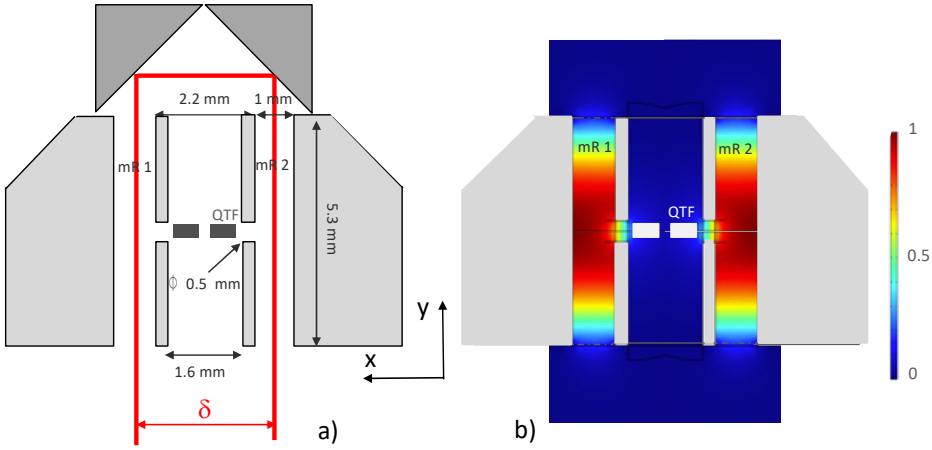

Figure 4. (**a**) Detailed dimensions of the monolithic double mR. The laser beam is represented in red. It is reflected by the right angle mirrors. (**b**) Normalized acoustic pressure generated into the double mR for f = 32,815 Hz, corresponding to the QTF resonant frequency.

The two mRs were accurately pre-positioned thanks to the monolithic design. They were spaced with a distance equal to the width of the QTF, plus an ideal gap of 70 µm on each side [15]. The two mirrors were glued onto a plate, thus setting an angle of 90° between the two reflective surfaces. The back plate slid along a shoulder in the back of the holder. Therefore, the two mirrors could be translated in the x direction, offering a simple mean of adjusting the distance between the in/out beams.

The setup was pre-aligned using a red laser. The visible laser was positioned instead of the IR laser and sent to mR 1. The mirrors were translated until the exiting beam consistently crossed mR 2. Next, the red laser was replaced by the IR laser and a focusing lens (f = 4 mm, Thorlabs C036TME-D). A power meter was used to monitor the output power. The exiting beam was sent to the power meter by using a tiny flat mirror, without cutting the incoming beam. The beam had to cross the 2 mRs without impinging their wall, meaning the beam size width had to be smaller than the mR radius over a distance ΔL equal to 2.2 cm. The laser was positioned about 20 cm far from the spectrophone to obtain a slowly converging beam. Using Gaussian optics and considering a beam waist of 1 µm at the laser output and the given lens, it could be shown that the laser beam could cross the double mR without any reflection. Approximately half of the initial optical power was measured at the output. This value could be mainly explained by the contribution of direct absorption by ambient water vapor (for a path length of 25 cm, and 50% RH, the power loss reached 36%). The remaining losses could come from reflections on the aluminum mirrors. An xyz translation stage was used to accurately position the QTF in between the mRs. The QTF resonance was measured by means of electronic excitation and used as a control signal during the descent inside the monolithic double mR setup. This continuous control technique was necessary to prevent the QTF collision and breakage. The frequency responses of the QTF, free and inside the mR, were compared, showing a Q factor of 14,140 and 9300, respectively (Figure 5). The Q value decrease (of about 30%) in this configuration was similar to the off-beam one. It was mainly due to the acoustic coupling between the QTF and mR [11]. The large signal offset observed in the characterization was due to the parallel capacitance of the coaxial cable connecting the transimpedance amplifier and could be easily suppressed. The parasitic capacitance could be suppressed by placing the amplifier closer to the QTF.

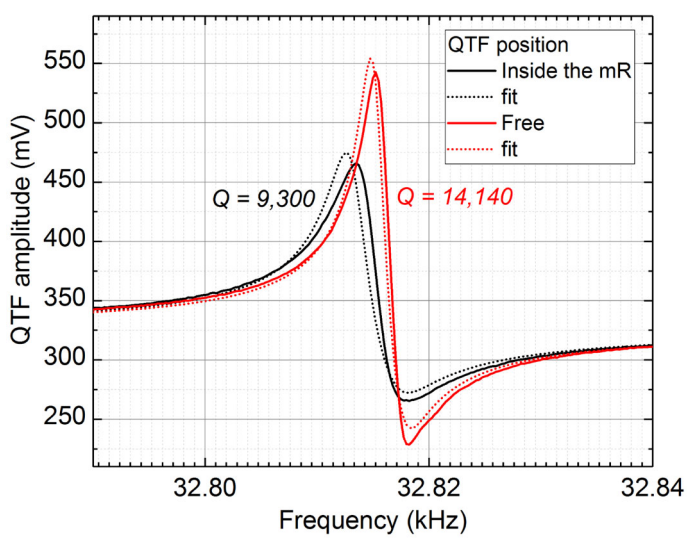

Figure 5. Frequency response of a QTF in free space (**red**) and positioned inside the double mR (**black**).

The Q factor was determined through the curve fitting with the Butterworth Von Dyke model.

3. Experimental Evaluation

The QTF was inserted in between the mRs, and the laser beam crossed the two mRs. The QEPAS signal was monitored as a function of the QTF position, in the y and z direction (Figure 6). The signal amplitude directly indicated the double mR-QTF coupling efficiency. In the z direction, the response grew significantly when the top of the prongs arrived in front of the slit and then decreased slowly as the lever became small. The response versus the y direction exhibited a mirror symmetry with the ordinate axis, and a maximum when y = 0, when the prong and the mR slit best overlapped.

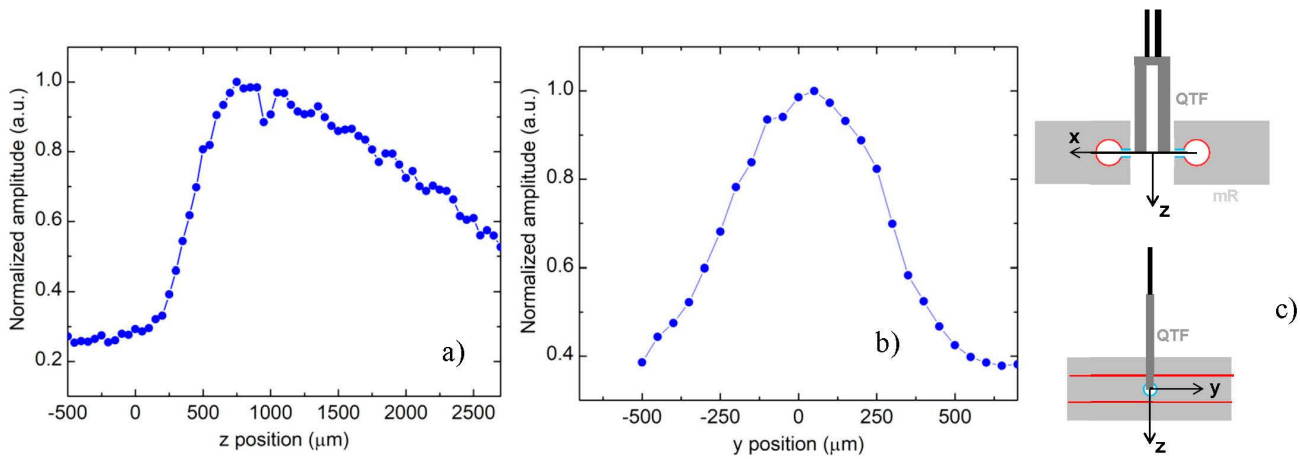

Figure 6. Evolution of the QEPAS signal when moving the QTF in the z (**a**) and y (**b**) direction. (**c**) Schematic of the mR and the QTF in the defined referential. The QTF is represented in the (0, 0, 0) position.

After the optimization of the QTF position, we studied the effect of each individual mR and compared it to the single off-beam configuration (with a single mR). To this end, we first measured the QEPAS signal as a function of the mirrors position. The mirrors were translated in the perpendicular direction with respect to the incoming beam, using a micrometric translation stage, thus changing the value of δ (Figure 1a). At first, the laser beam only crossed the mR 1, giving a QEPAS signal maximum of about 20 mV (Figure 7). When the mirror was translated, the beam crossed the mR 2 and the signal rose to 40 mV, doubling the initial value of the signal. The signal presented a plateau over 200 μm. The results could also be presented in terms of the QEPAS signal versus the laser current, with the typical 1*f* signal shape (Figure 7b). We added the signal obtained with the conventional off-beam, whose amplitude was about 30 mV. The amplitude difference between the off-beam and the misaligned monolithic double mR setup was associated with the mR resonance. In the off-beam configuration, the slit was considered almost open while in the double mR configuration, the slit should be considered as almost closed, thus changing the acoustic resonant frequency.

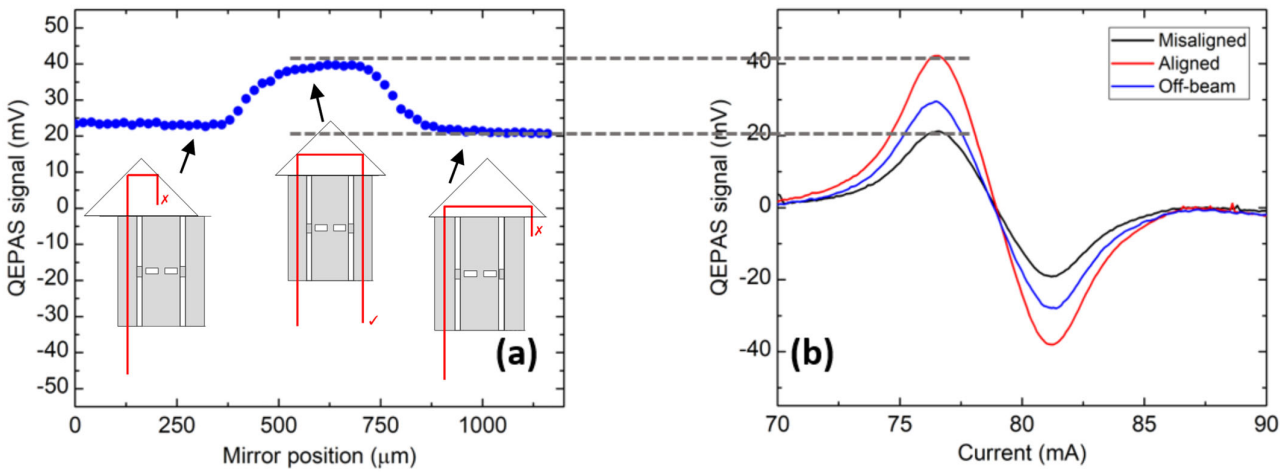

Figure 7. (**a**) Effect of the mirror position on the QEPAS signal maximum. (**b**) QEPAS signal versus laser current when the beam is misaligned (**black**) or aligned (**red**) with the mR 2, and comparing it with the results from conventional off-beam (**blue**).

Hu [16,17] made a thorough study on the effect of the length and the radius of the mR. The optimized spectrophone showed a Signal to Noise Ratio (SNR) gain of ≈20 and ≈40, without and with the right-angle mirror, respectively, which corresponded to a two-factor increase, in good agreement with the results obtained in this paper.

We eventually estimated the normalized noise equivalent absorption (NNEA) on a 1f QEPAS signal in the double mR configuration (Figure 8a). We calculated the Allan-Werle deviation (Figure 8b). For the given relative humidity and ambient temperature, the absolute water vapor concentration in ambient air was 9900 ppmv (40% RH, 20 °C). The long-term drift appeared after a few seconds but the signal was really clean. The limit of detection was 2 ppmv in 1 s, giving an NNEA of 1.2×10^{-8} W·cm^{-1}·Hz$^{-0.5}$.

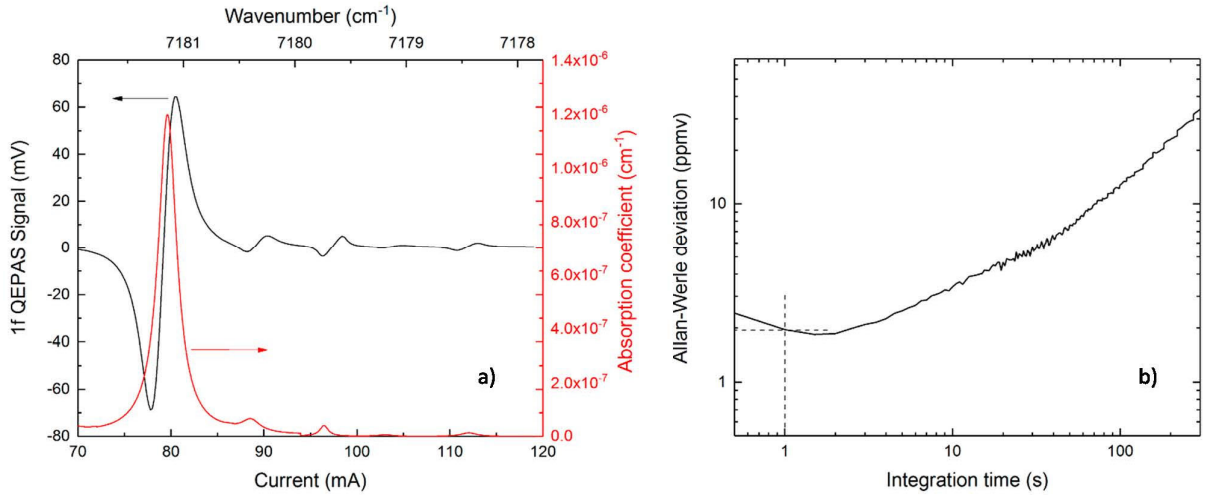

Figure 8. (**a**) 1f optimized double mR QEPAS signal (black). In red, the HITRAN database [18] absorption coefficient of the gas line (1ppmv) is reported. (**b**) Allan-Werle deviation calculated from a 15 nm acquisition of the 1f QEPAS signal.

The NNEA in this absorption range was comparable to a previously published paper [12] on water sensing, with a T-shape off-beam configuration. Even if the double mR 1f signal was clean, the long-term drift appeared sooner than in the QEPAS systems

using closed cells. This value might be improved using a more stable configuration, with an enclosed gas cell.

4. Conclusions

A novel design was proposed, using 2 mRs in a monolithic setup, to increase the acoustic pressure actuating on the two external sides of QTF prongs. The double mR was 3D printed, showing the ability and flexibility of the stereolithography method in printing small and complex parts.

While off-beam configuration might be less sensitive than on-beam, its advantages on the laser beam alignment and physics phenomena decoupling, offers many interests. The double mR spectrophone combine these advantages with a better acoustic excitation, thus, there is an increased value of the QEPAS signal. The strength of the double mR method relies on the large enhancement of the mR and QTF coupling. The surface of the prong was normal to the wave propagation direction, thus the acoustic pressure efficiently actuated the QTF. The weakness of the technique was the sensitivity to the QTF positioning, compared to the conventional off-beam. However, the required spatial accuracy (10–30 μm) was definitely reachable, using micropositioners.

The gap between the 2 mRs was adjusted at the printing level, simplifying the process of the QTF positioning. An enhancement could be obtained by adjusting the mRs dimensions to better fit the QTF frequency. It would be interesting to evaluate the use of custom QTF [9,19] specifically developed to enhance coupling due to an external prong excitation. Finally, the high-resolution 3D-printing should be considered in the design of acoustic resonant cells, such as Helmholtz configurations coupled with mechanical resonators.

Author Contributions: R.R. was in charge of the methodology, the software, and the investigation, under the supervision of A.V. He was assisted by D.A., N.M., and W.T. for data curation. The article was written by R.R. and A.V., reviewed and edited by M.B. and A.V. All authors have read and agreed to the published version of the manuscript.

Funding: This research was funded by ANR MULTIPAS project (ANR-16-CE04-0012). It was partially supported by the French "Investment for the Future" program: EquipEx EXTRA, (ANR-11-EQPX-0016) and Montpellier University MUSE SENSIR project (ANR-16-IDEX-0006).

Informed Consent Statement: Not applicable

Institutional Review Board Statement: Not applicable

Conflicts of Interest: The authors declare no conflict of interest.

References

1. Kosterev, A.A.; Bakhirkin, Y.A.; Curl, R.F.; Tittel, F.K. Quartz-enhanced photoacoustic spectroscopy. *Opt. Lett.* **2002**, *27*, 1902–1904, doi:10.1364/OL.27.001902.
2. Köhring, M.; Böttger, S.; Willer, U.; Schade, W. LED-absorption-QEPAS sensor for biogas plants. *Sensors* **2015**, *15*, 12092–12102, doi:10.3390/s150512092.
3. Palzer, S. Photoacoustic-based gas sensing: A review. *Sensors* **2020**, *20*, 2745, doi:10.3390/s20092745.
4. Weidmann, D.; Kosterev, A.A.; Tittel, F.K.; Ryan, N.; McDonald, D. Application of a widely electrically tunable diode laserto chemical gas sensing with quartz-enhanced photoacoustic spectroscopy. *Opt. Lett.* **2004**, *29*, 1837–1839, doi:10.1364/OL.29.001837.
5. Liu, K.; Guo, X.; Yi, H.; Chen, W.; Zhang, W.; Gao, X. Off-beam quartz-enhanced photoacoustic spectroscopy. *Opt. Lett.* **2009**, *34*, 1594–1596, doi:10.1364/OL.34.001594.
6. Dong, L.; Kosterev, A.A.; Thomazy, D.; Tittel, F.K. QEPAS spectrophones: Design, optimization, and performance. *Appl. Phys. B* **2010**, *100*, 627–635, doi:10.1007/s00340-010-4072-0.
7. Yi, H.; Chen, W.; Guo, X.; Sun, S.; Liu, K.; Tan, T.; Zhang, W.; Gao, X. An acoustic model for microresonator in on-beam quartz-enhanced photoacoustic spectroscopy. *Appl. Phys. B* **2012**, *108*, 361–367, doi:10.1007/s00340-012-4988-7.
8. Borri, S.; Patimisco, P.; Sampaolo, A.; Beere H.E.; Ritchie, D.A.; Vitiello, M.S.; Scamarcio, G.; Spagnolo, V. Terahertz quartz enhanced photo-acoustic sensor. *Appl. Phys. Lett.* **2013**, *103*, 021105, doi:10.1063/1.4812438.
9. Patimisco, P.; Sampaolo, A.; Zheng, H.; Dong, L.; Tittel, F.K.; Spagnolo, V. Quartz–enhanced photoacoustic spectrophones exploiting custom tuning forks: A review. *Adv. Phys. X* **2017**, *2*, 169–187, doi:10.1080/23746149.2016.1271285.

10. Yi, H.; Liu, K.; Sun, S.; Zhang, W.; Gao, X. Theoretical analysis of off beam quartz-enhanced photoacoustic spectroscopy sensor. *Opt. Commun.* **2012**, *285*, 5306–5312, doi:10.1016/j.optcom.2012.07.056.
11. Liu, K.; Yi, H.; Kosterev, A.A.; Chen, W.; Dong, L.; Wang, L.; Tan, T.; Zhang, W.; Tittel, F.K.; Gao, X. Trace gas detection based on off-beam quartz enhanced photoacoustic spectroscopy: Optimization and performance evaluation. *Rev. Sci. Instrum.* **2010**, *81*, 103103, doi:10.1063/1.3480553.
12. Yi, H.; Chen, W.; Sun, S.; Liu, K.; Tan, T.; Gao, X. T-shape microresonator-based high sensitivity quartz-enhanced photoacoustic spectroscopy sensor. *Opt. Express* **2012**, *20*, 9187–9196, doi:10.1364/OE.20.009187.
13. Rück, T.; Bierl, R.; Matysik, F. NO_2 trace gas monitoring in air using off-beam quartz enhanced photoacoustic spectroscopy (QEPAS) and interference studies towards CO_2 , H_2O and acoustic noise. *Sens. Actuators B Chem.* **2018**, *255*, 2462–2471, doi:10.1016/j.snb.2017.09.039.
14. Maurin, N.; Rousseau, R.; Trzpil, W.; Aoust, G.; Hayot, M.; Mercier, J.; Bahriz, M.; Gouzi, F.; Vicet, A. First clinical evalua-tion of a quartz enhanced photo-acoustic CO sensor for human breath analysis. *Sens. Actuators B Chem.* **2020**, 128247, doi:10.1016/j.snb.2020.128247.
15. Rousseau, R.; Loghmari, Z.; Bahriz, M.; Chamassi, K.; Teissier, R.; Baranov, A.N.; Vicet, A.Off-beam QEPAS sensor using an 11-μm DFB-QCL with an optimized acoustic resonator. *Opt. Express* **2019**, *27*, 7435–7446, doi:10.1364/OE.27.007435.
16. Hu, L.; Zheng, C.; Zheng, J.; Wang, Y.; Tittel, F.K. Quartz tuning fork embedded off-beam quartz-enhanced photoacoustic spectroscopy. *Opt. Lett.* **2019**, *44*, 2562, doi:10.1364/OL.44.002562.
17. Hu, L.; Zheng, C.; Zhang, M.; Yao, D.; Zheng, J.; Zhang, Y.; Wang, Y.; Tittel, F.K. Quartz-enhanced photoacoustic spectroscopic methane sensor system using a quartz tuning fork-embedded, double-pass and off-beam configuration. *Photoacoustics* **2020**, 100174, doi:10.1016/j.pacs.2020.100174.
18. Gordon, I.E.; Rothman, L.S.; Hill, C.; Kochanov, R.V.; Tan, Y.; Bernath, P.F.; Zak, E.J. The HITRAN2016 molecular spectroscopic database. *J. Quant. Spectrosc. Radiat. Transf.* **2017**, *203*, 3–69, doi:10.1016/j.jqsrt.2017.06.038.
19. Duquesnoy, M.; Aoust, G.; Melkonian, J.M.; Lévy, R.; Raybaut, M.; Godard, A. Quartz enhanced photoacoustic spectroscopy based on a custom quartz tuning fork. *Sensors* **2019**, *19*, 1362, doi:10.1080/23746149.2016.1271285.